Cement & Concrete Composites 39 (2013) 73–81

Contents lists available at SciVerse ScienceDirect

Cement & Concrete Composites

journal homepage: www.elsevier.com/locate/cemconcomp

Mechanical properties of photocatalytic white concrete subjected to high temperatures

Luigi Biolzi [a], Giovanni Di Luzio [a,*], Joseph F. Labuz [b]

[a] Department of Structural Engineering, Politecnico di Milano, Milan, Italy
[b] Department of Civil Engineering, University of Minnesota, Minneapolis, MN, USA

ARTICLE INFO

Article history:
Received 1 November 2012
Received in revised form 20 March 2013
Accepted 22 March 2013
Available online 6 April 2013

Keywords:
High performance white concrete
Thermal treatment
Thermal damage characterization
Mechanical properties degradation
Size effect

ABSTRACT

The paper describes the consequences of progressive damage in architectural high performance concrete when exposed to different heating treatments. Specimens were tested for uniaxial compressive, direct, and indirect tensile strengths at ambient conditions approximately one day after the exposure to the high temperature. Modifications in the microstructure, porosity, and pore size distribution of the fire deteriorated specimens were identified using scanning electron microscopy and mercury intrusion porosimetry techniques. Test results revealed no significant variations in the mechanical strengths for specimens exposed to temperatures up to 250 °C. Per contra, significant damage was observed for higher temperature, 500 °C and 750 °C, treatments, similar to that of ordinary concrete made with similar aggregates. Based on X-ray diffraction analysis, photocatalytic properties of the concrete were lost at 750 °C.

1. Introduction

The behavior of concrete exposed to transient temperature conditions and mechanical loading has been comprehensively investigated, particularly under actions such as high temperatures from fire [1,2]. Normal concrete is flameproof and reveals good resistance to fire, though it is not considered as a refractory material. Heating to high temperature generates modification to the mineralogy and fabric of the material, with chemical/physical transformations in aggregates and paste, and possible increase of small pores and microcracks within the concrete element. These alterations are dependent on the maximum temperature reached, the length of time at that temperature, and the rate of heating and cooling [3]. The effects of damage are in the form of cracking, spalling, discoloration, and dehydration of calcium hydroxide and other cementitious phases [4,5]. Internal microcracking usually occurs within the cement paste, around, and across aggregate particles, accompanied by deformation [5]. The progress of concrete technology led to high performance concretes, and the behavior under high temperatures, primarily for high strength concretes, is explosive spalling. The dense microstructure of high strength concrete compared to normal concretes impedes the moisture transport out of the specimen. As a result, the internal vapor pressure increases, promoting the explosive spalling [6].

Microcracking in concrete reduces the material stiffness and strength. As the number and/or size of the microcracks increase, there is a corresponding decrease in the mechanical properties. In addition, microcracks respond differently under tension and compression, and the resulting effective moduli of microcracked concrete will differ depending upon the magnitude and direction of the applied loads. Microcracking and the consequent changes produced in the material structure can have a significant effect on the overall structural response to loads [7]. The prediction of these changes can be used to explain the damage evolution process in a quasi-brittle material such as concrete. In particular, microcracks have a significant impact on the true residual strength of the material, and it is necessary to properly analyze the influence of a given specimen size on the experimental data, e.g. when evaluating the nominal strength [8].

In this paper, the consequences of progressive damage in a white high performance concrete containing titanium dioxide (TiO_2), and possessing photocatalytic properties when exposed to different heating treatments, are investigated. Exploiting TiO_2 photocatalysis in the concrete means having a self-cleaning effect of building facades, a retardation of natural surface ageing as well as depollution of air [9]. The concrete specimens were thermally treated at temperatures of 250, 500, and 750 °C in an electrical radiant oven. No explosive spalling was observed in any specimen during the treatment. Residual property tests [10] were monitored with an interferometric technique referred to as electronic speckle pattern interferometry, which provides a map of the displacement field. After the mechanical tests, concrete samples were submitted

* Corresponding author. Tel.: +39 0223994278.
E-mail address: diluzio@stru.polimi.it (G. Di Luzio).

0958-9465/$ - see front matter © 2013 Elsevier Ltd. All rights reserved.
http://dx.doi.org/10.1016/j.cemconcomp.2013.03.016

Table 1
Mix proportions.

White cement TX Arca 42,5 R	500 kg/m^3
Metacaolin	40 kg/m^3
Aggregate five fractions, 0–10 mm	1650 kg/m^3
Acrylic superplasticizer	1.85% (cement content)
Water/cement ratio	0.46

to physicochemical characterization and microscopic observations. In addition, X-ray diffraction techniques were also used to analyze the changes of the hydration products.

2. Experimental techniques

2.1. Mix designs and test specimens

Mix-components of the cement-based materials used for this investigation are summarized in Table 1. The aggregate was crushed marble with a maximum nominal size of 10 mm. An acrylic superplasticizer, a polymer of polyacrylic acid sulfonate based (formaldehyde free), was used at a dosage of 1.85% of cement content to achieve the desired workability. After casting, the specimens were covered with wet burlap under a polyvinyl sheet. After 24 h, the specimens were removed from the mold and cured under lime-saturated water at a temperature of 20 ± 2 °C.

2.2. Heating procedure

Thermal load was applied by means of a computer-controlled radiant electric furnace. The furnace of power 15 kW, consisting of a 400 × 700 × 1300 mm (width × height × length) inner chamber lined with refractory material, generates a maximum temperature of 1000 °C. The upper part, which is removable through a hoisting crane, contains the heating elements and thermocouples. The lower part is used for positioning the specimens, leaving adequate space between them, both horizontally and vertically, to ensure a uniform heat treatment. The heating patterns employed in the experiments are shown in Fig. 1. The control system can be programmed to realize linear heating curves, target temperatures of 250, 500, and 750 °C and a time when it must be achieved, a holding time (2.5 h) at constant temperature, and a final cooling time.

2.3. Experimental set-up

The testing system used for tensile tests consisted of a closed-loop electromechanical Instron load frame with a maximum capacity of 100 kN. To avoid unstable failure, strain control tests were performed with the choice of crack mouth opening displacement as the feedback signal to the servo-controller [11].

In order to identify the crystal phases in the different samples, X-ray diffraction (XRD) analysis was performed. The data were collected using a Philips PW 1820 diffractometer employing CuKa radiation (λ_0 = 1.54 Å).

Several specimens were selected to perform microscopic observations. Abrasive wet-cutting was practiced to prevent damaging the specimens. Specimens used for the scanning electron microscope were encapsulated in an epoxy resin. After the hardening of the resin, the samples were polished with diamond pastes. In order to remove any residual polishing compound, a cleaning with ethanol was carried out. The samples were coated with carbon to provide a conductive surface for SEM observations with LEO 1450 VP Scanning Electron Microscope.

The electronic pattern speckle interferometry (ESPI) is an interferometric method used to measure a deformation field of diffusely scattering objects. ESPI is full field strain measurement technique. When an optically rough surface is illuminated by a laser beam, a random pattern of irregular or regular dots is observed. This phenomenon is called a laser speckle pattern. In this technique, two laser beams are used to illuminate the object, so that, by combining the object speckle and the reference beam, it is possible to obtain a brightness of the image speckle very sensitive to specimen movement.

3. Experimental results

3.1. Concrete properties

Fresh and hardened properties of concrete were assessed at room temperature and are shown in Table 2. The specimens were removed from the molds after 24 h, then cured in water at 20 °C for at least 28 days before testing.

3.2. X-ray diffraction (XRD)

According to the XRD analysis, it is possible to evaluate the evolution of damage in concrete, as a function of the mineralogical changes on heating. The cement hydrates in the hardened concrete bulk, undergoing a progressive loss of water (free water initially, bound water over 200 °C). When the temperature of the paste reaches 400 °C, there is a progressive transformation of calcium hydroxide (dehydroxylation) until its complete disappearance (near 650–700 °C). This is also observed in terms of C_3S, which is progressively reduced until its transformation into C_2S (at 750 °C). Ettringite, which was observed until a treatment

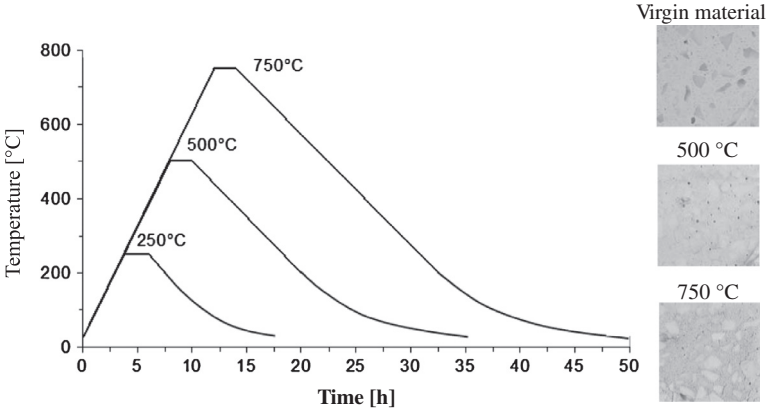

Fig. 1. Thermal treatment of concrete specimens.

Table 2
Fresh and hardened properties of concrete.

Fresh properties			
Slump flow [mm]	Time flow [s]		Air content [%]
500	3.5		2.8
Hardened properties			
Density [kg/m^3]	f_c' [MPa]	f_t [MPa]	E [GPa]
2350	66.5	5.50	32.4

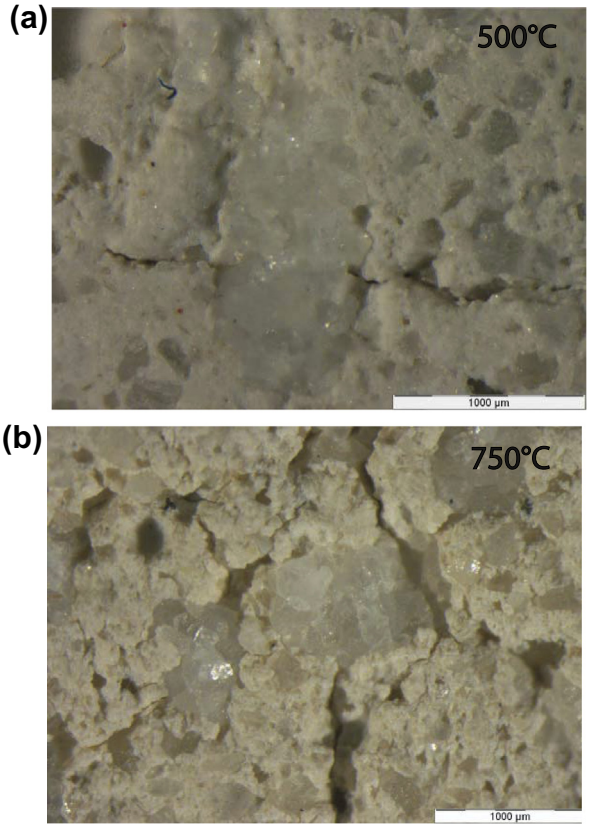

Fig. 2. SEM observations of white concrete treated at (a) 500 °C and (b) 750 °C.

temperature of 250 °C, disappears when 500 °C is reached. At higher temperatures (750 °C), there is the titanium dioxide (TiO_2) phase transformation from anatase to rutile, the formation of $\alpha' C_2S$ and periclase (Mg oxide) in place of dolomite (Ca–Mg carbonate). These mineralogical changes correspond to a parallel loss in strength, which is evident for temperatures greater than 500 °C. From the point of view of thermal deformation of the concrete phases, it is well known that a cement paste shrinks due to the loss of hydrates. This effect cannot be counterbalanced by the thermal expansion of aggregates, so the final result is shrinkage induced progressive cracking of the material, mainly involving the paste, the interface between paste and aggregates, and finally (at higher temperatures) the aggregate itself.

3.3. Scanning electron microscope (SEM)

SEM investigations showed distinct changes in the morphology as a consequence of exposure to high temperatures. Micrographs that reveal characteristic features of the undamaged materials after the exposure are shown in Fig. 2. The different thermal behavior of the different components of concrete, when exposed to high temperature, generates microcracks and other defects within the material. The most affected regions are associated with the aggregate and the cement paste. Both the cement paste and the aggregate are affected by chemical processes that cause stresses within the material due to thermal incompatibility. A fairly large number of microcracks were observed in the specimens with a single cycle up to 500 °C (Fig. 2a). A much higher crack density was detected in the specimens exposed to 750 °C (Fig. 2b), revealing serious changes in the morphology, characterized by diffuse microcracks across both the aggregate and cement paste. The increase in microcracking was confirmed by examining the increased permeability and reduced mechanical properties.

3.4. Porosity

Porosimetric data – cumulative volume (cm^3/g) and total porosity (%) – are summarized in Fig. 3. A significant increase in porosity was observed after heating at 750 °C, confirming an enhanced material degradation that can have an effect on the mechanical properties. In particular, with reference to undamaged concrete, the porosity values more than doubled with a thermal treatment up to 750 °C.

3.5. Ultrasonic pulse velocity (UPV)

The UPV value, a supplementary indicator of damage, has been used effectively to estimate the quality of concrete, as UPV is sensitive to degradation phenomena including internal cracking [12]. From the value of 4140 m/s for the virgin material, the UPV value, after treatment of 250 °C, decreases almost linearly as the maximum heating temperature increases. Note that velocities of around 3100 m/s were measured after a single cycle up to 250 °C, but values around 1050 m/s were measured in specimens heated to 750 °C. As expected, Young's modulus of the concrete exhibits a similar trend, with a monotonically decrease with increasing temperature above 250 °C.

3.6. Residual nominal strength

Tensile Loading: the direct tensile test has several limitations, including the testing system itself (control and boundary conditions) and the specimen geometry (prismatic or dog-bone shape). In particular, the choice of the feedback signal for uniaxial tension of a prismatic specimen is obvious, although the placement of the transducer is not, as the crack can form anywhere through the section. For this reason, a gradual reduction of the cross-section–the dog-bone shape–fixes the location of the crack. The fabrication of this geometry, however, poses a significant machining effort. A compromise solution is to introduce notches, which produce an abrupt change of the cross-sectional area and a perturbation of the stress field.

It is possible to perform a uniaxial test with different constraints [13,14]: rotating platens that allow bending or fixed platens that impose a uniform displacement. A fundamental issue of rotating platens is the problem of specimen alignment with the grips, which may induce biaxial bending that promotes localization and fracture. Even with near perfect centering, experiments show that the peak load is reached with localization of deformation only on one side of the specimen [15]. A single crack, formed in this localized region, is usually observed extending from one side. As a result, there is bending of the specimen that leads to a strong perturbation in the homogeneous stress field. A clear non-uniform crack growth through the critical cross section of the specimens is typically detected.

With a fixed platens loading system (Fig. 4), it is possible to impose an almost symmetric crack propagation pattern; the crack commonly starts on one side, but the kinematic condition imposes

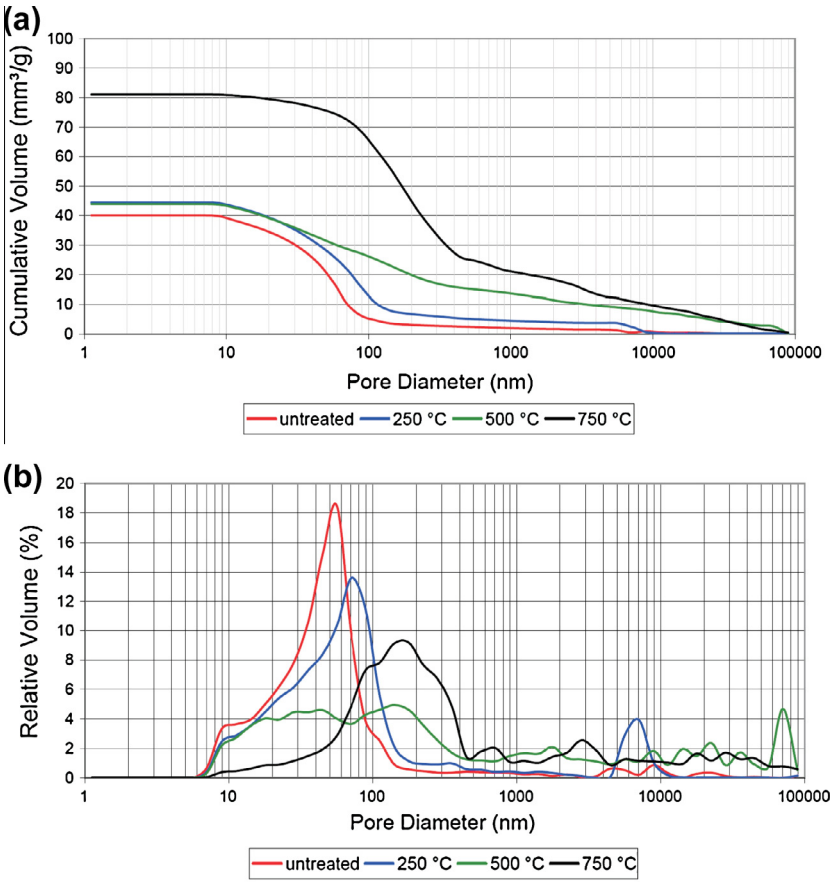

Fig. 3. Porosity results: (a) cumulative volume and (b) total porosity vs pore diameters.

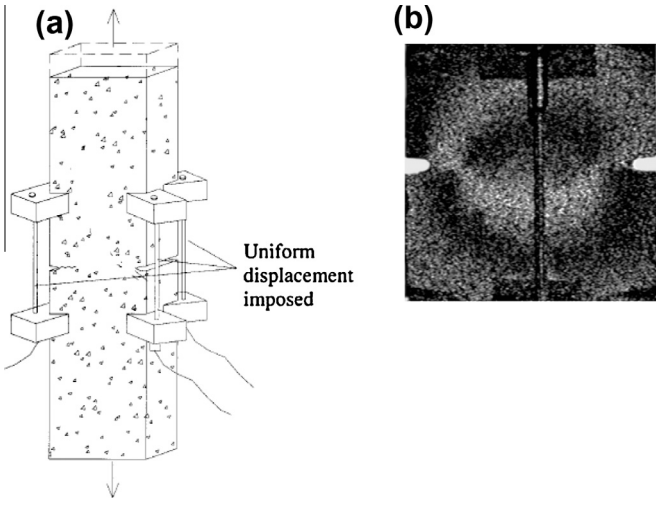

Fig. 4. Tensile tests: (a) experimental set up and (b) ESPI image at peak load.

the growth of a second crack on the other side. By continuous displacement control, the two cracks advance simultaneously across the specimen until complete failure (Fig. 4b).

Tension tests were performed with the fixed platens condition and the load-point displacement was measured at four locations by four LVDTs. These four sensors were used to ensure a uniform displacement around the four specimen corners. The specimens, 40 mm thick, 200 mm long and 50 mm wide, were notched to a relative depth of 0.1 (the ratio between the notch length and specimen width), with the added benefit of maintaining control into the post-peak regime. The tests were performed at a displacement rate of 5×10^{-6} mm/s. The average value of displacements measured using two LVDTs, with a sensitivity of 0.2 mm/v, set across the notch at a gage length of 50 mm, was used. The specimen was carefully glued to the plates clamped to the testing machine, making the geometrical tolerance between the specimen and plates very small.

A comparison of the different mean responses recorded with the four LVDTs mounted around the specimens is shown in Fig. 5a. The symmetry with fixed platens was enforced and maintained along the overall loading process without any lateral flexing (transverse displacement) of the specimen, as monitored by the four LVDTs. Fracture initiation and propagation were symmetric. Fig. 5b shows the tensile strength as a function of the maximum temperature of the thermal cycles. While it is impossible experimentally to maintain the symmetric propagation of a center-cracked specimen, the double symmetry can be realized with the modified load frame and the double-notched specimen. The eccentricity from the imperfections can be eliminated by the adjustable dynamometric bars. Thus, an estimate of the tensile strength can be obtained without significant perturbation of the stress field.

Bending Tests: to determine the fracture properties under various heating scenarios, three-point bending (3PB) tests were also performed on preheated concrete beams of dimensions $600 \times 200 \times 50$ mm (L-specimens), $300 \times 100 \times 50$ mm (M-specimens) and $150 \times 50 \times 50$mm (S-specimens). The effective span of the beams was 560 mm, 280 mm and 150 mm, respectively; the notch length was $0.2D$ (D is the section height) and 3 mm wide. Typical bending stress–displacement curves for specimens of larger dimensions for a given thermal cycle are shown in Fig. 6.

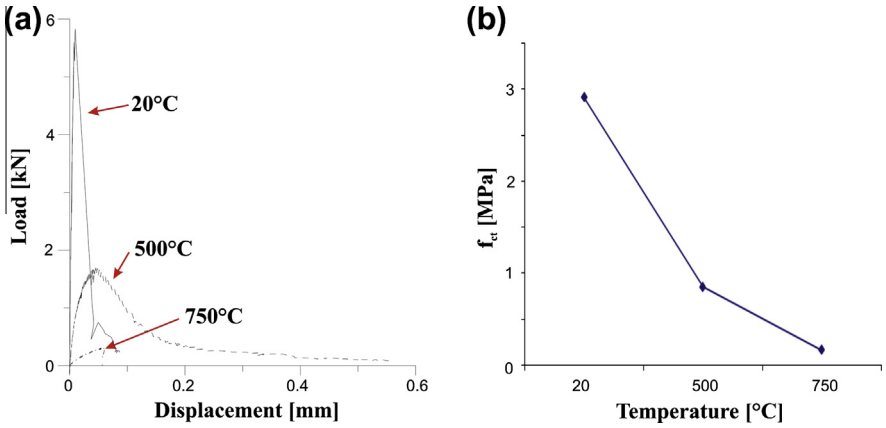

Fig. 5. Tensile tests: (a) load vs displacement curves and (b) tensile strength vs treatment temperature.

Softening is apparent with increasing temperature. The nominal stress for bending can be computed from the flexure formula:

$$\sigma_N = \frac{M_{max}}{S} \tag{1}$$

where $M_{max} = P_{max}L/4$ is the maximum moment at peak load (P_{max}), L is the length of the span, $S = D^2b/6$ is the elastic section modulus, and b is the thickness.

The values of the nominal stresses are shown in Fig. 7 as a function of the maximum temperature of the thermal cycles. For the range of temperatures considered in this study, all bending strengths underwent a two-stage process. In the first stage, these strengths either changed very little or slowly decreased with temperature until a transition point was reached. In the second stage, the strengths rapidly decreased with the severity of thermal treatment. This transition point is around 250 °C. For the considered materials, the concrete bending strengths change little at the lower temperatures and consequently, during this physical process, the removal of capillary water would not cause a significant reduction in strength. There is no change up to a temperature of 300 °C in aggregate and mortar phases, but there are significant changes in aggregate and mortar phases above this temperature.

Compressiveloading: all tests were carried out on cubic specimens of 100 mm and 200 mm side, and were cured under water at room temperature until test time. Before testing, the specimens were removed from the curing tank and the ends were ground to be plane and perpendicular. The experimental results are summarized in Fig. 8. Similar to bending strength, creation of pores and cracks resulting from physicochemical changes in cement paste and thermal incompatibility between aggregate and cement paste caused a deterioration in compressive strength, although the failure mode in uniaxial compression is more complex than three-point bending.

3.7. Material stiffness

The thermally damaged/cracked medium responds differently under tensile and compressive loads as microcracks open or close, hence there are different Young's moduli and bulk moduli under tension and compression loading. To determine elastic moduli, strain gages measurements were used after the treatment at various temperatures, and Fig. 9 illustrates the elastic moduli as a function of the maximum temperature. The trends show that moduli for the concrete decrease. However, the ratio of reduction for the elastic moduli is different under tension and compression. In particular, there is a sharp reduction at 250 °C and a gradual decay in the temperature range of 250–750 °C. It should be remarked that, as a consequence of damage, the significant reduction of

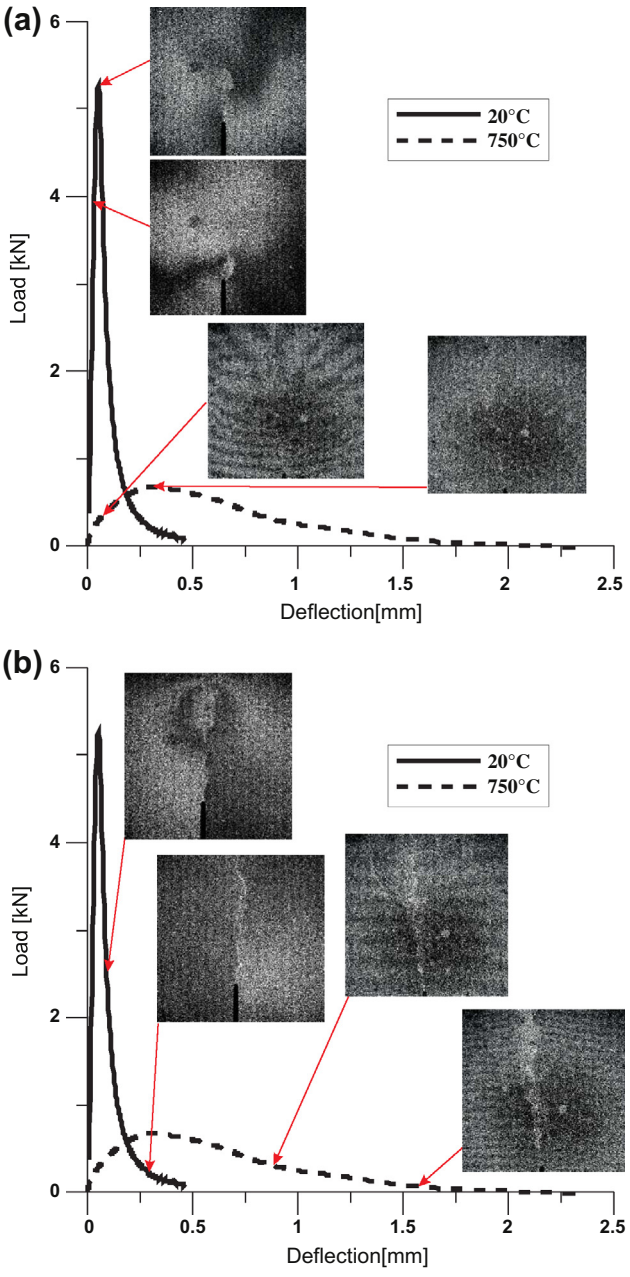

Fig. 6. Experimental results of bending tests: typical load deflection curves and ESPI images at (a) pre and (b) post peak.

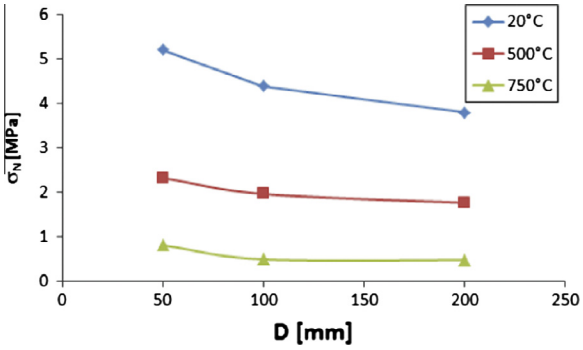

Fig. 7. Dependence of modulus of rupture on specimen size and heat treatment.

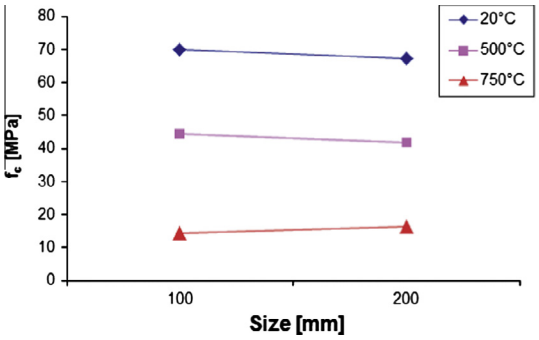

Fig. 8. Dependence of uniaxial compressive strength on specimen size and heat treatment.

strength and stiffness after exposure to elevated temperatures is obvious, but the trends in strengths and moduli decay are different.

3.8. ESPI analysis

A comparison between the ESPI observations (Figs. 6 and 10c) shows the evolution of damage due to the thermal treatment. ESPI images detected in specimens thermally treated with a single cycle at 250 °C are not included because their differences with the ones noticed in undamaged concrete were insignificant. Localization was visible with ESPI prior to peak load (Fig. 6a) and fracture was noticed at various stages of growth (Fig. 6b). A comparison among the ESPI images included in Fig. 6 clearly shows that, at peak load, the thermal damage alters the strain field. The ESPI images indicate that the size of the process zone was strongly influenced by the damage, which causes local heterogeneity of the material. The experimental evidence clearly showed that, due to thermal treatment, the strain field at peak load was perceptibly different in the specimens, and in particular, in the critical cross section, where the coalescence of microcracks leads to the formation of the main fracture. For the specimens heated up to 750 °C, the ESPI images show that the region of localized deformation was much more extended in length and width. Thus, the stress distribution was altered due to the microstructural differences (increased heterogeneities) generated in the material, and the phenomenon of thermal damage in concrete appears, from a fracture mechanics point of view, as a problem where the width of the damage zone grows. As a consequence, the material and the structural ductility increase.

In the specimens damaged at 750 °C, the ESPI images showed a neutral axis considerably moved towards the upper part of the specimen, that is, the tensile region appeared considerably increased. This is further evidence of the significant difference of elastic moduli in tension and compression. Indeed, assuming plane sections remain plane, the strain is proportional to the distance from the neutral axis. As the axial force is zero, the resultant of the normal stresses must vanish. From these conditions in the elastic regime, the position of the neutral axis is given by the distance from the upper side of the cross-section $k\,D$, with the factor k larger than zero but smaller than one:

$$k = \frac{1}{1 + \sqrt{E_C/E_T}} \tag{2}$$

where E_C and E_T represent the Young's modulus for compressive and tensile load, respectively. For the virgin material ($E_C = E_T$), k is equal to 0.5. For concrete treated at 750 °C ($E_C = 9E_T$), k is equal to 0.25. This is confirmed by the ESPI images in Fig. 10a and b for the virgin material and concrete treated at 750 °C, respectively, for 3PB tests with unnotched specimens.

4. Discussion

Nondestructive (ESPI, XRD, ultrasonic pulse velocity, SEM, porosimetric analysis) and destructive experiments were used to investigate damage phenomena associated with exposure to high temperatures. The white architectural concrete considered satisfies both aesthetic and structural requirements. The coloration of the material remained unchanged with thermal treatment, ensuring that the aesthetic demands were observed; i.e. elevated temperatures did not cause significant changes in color, at least for a temperature up to 750 °C. The heat treatment affects the internal stress field and, due to physical and chemical transformations occurring in the material and different thermal expansion coefficients of its components, microcracking was detected. In specimens treated up to 500 °C, SEM images showed cracking of the concrete distributed randomly along the edges, in the interfacial zones between the cement paste and aggregate. In specimens treated up to 750 °C, microcracks were more widespread and of larger dimensions in comparison to the specimens treated at 500 °C. The different thermal behavior of the components caused a diffuse separation of the aggregate from the cement paste.

The test results of porosimetric mercury intrusion highlight the fact that the pores present in the 750 °C specimens had a larger diameter than the 500 °C, and with respect to the 250 °C and reference material (untreated) specimens as well. The cumulative volume of pores was 80 mm^3/g for the 750 °C specimens and 45 mm^3/g for 500 °C. Analyzing the overall test results and those obtained from porosimetric observation of the SEM images, it appeared that the material at 750 °C had suffered significant damage compared to specimens heated to 500 °C. The porosimetric results of tests on specimens treated at 250 °C showed similar values as the reference (virgin) specimens. At these temperatures, no chemical processes produced expansion but only a loss of water. Thus, the damage was not significant.

The uniaxial compressive strength of specimens 250 °C, 500 °C, and 750 °C is respectively 88%, 60%, and 22% of the reference material. The uniaxial tensile strength of the reference material is 2.90 MPa, while the specimens treated at high temperatures exhibited strength 30% (500 °C) and 5% (750 °C) of the virgin material. With increasing severity of damage as temperature is increased, the uniaxial compressive:tensile strength ratio increases.

With increasing temperature of the heat treatment, the material has a different behavior in tension and compression, as measured by the Young's moduli. For the virgin material, the values of Young's moduli were almost identical; the material had the same stiffness in compression and tension. The heat treatments induced microcracking that progressively affected the material stiffness differently in compression, where the microcracks tended to close, as

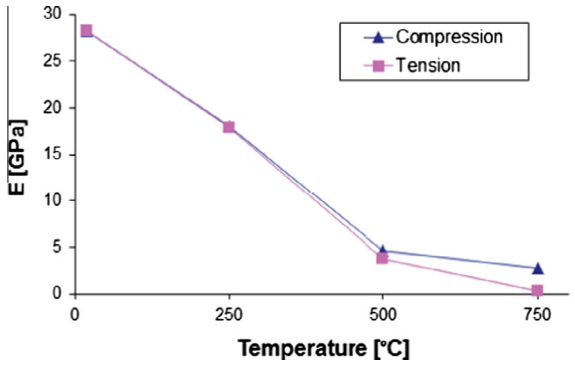

Fig. 9. Dependence of Young's modulus on heat treatment and loading type.

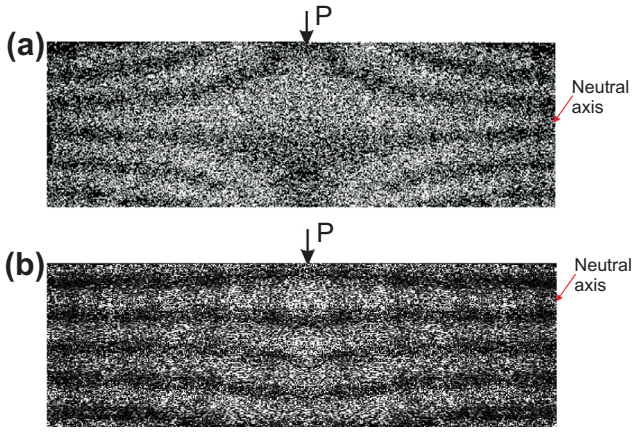

Fig. 10. ESPI images from 3 PB tests in the elastic regime for (a) virgin concrete and (b) concrete thermally treated at 750 °C.

Table 3
Nominal strength of TPB tests for concrete after different thermal treatment.

D[mm]	Ref. σ_N (MPa)	500°C σ_N (MPa)	750 °C σ_N (MPa)
50	2.76	1.32	0.325
100	2.57	1.17	0.294
200	2.28	1.09	0.293

opposed to tension, where a reduction of stiffness is due to opening of microcracks. The higher the temperature of the treatment, the greater the difference between Young's modulus in compression and tension. For example, specimens treated at 750 °C exhibited a modulus value ten times lower than the virgin material. Of course, the reason for the degradation is microcracking, which is also the cause of the shift in the neutral axis. In the thermally damaged specimens, the neutral axis tends to move towards the upper (compression) side of the cross-section, as shown by the ESPI monitoring. The position depends on the severity of the thermal treatment.

Unlike strength, Young's modulus is much influenced by the process of removal of capillary water, which occurs in the early stages of heating. This can be seen by comparing the decay of Young's modulus and uniaxial compressive strength: the modulus in compression of 250 °C is 60% compared to the undamaged material, 16% for 500 °C, and 9% for the 750 °C. The modulus was already penalized after a thermal treatment at 250 °C, at which point mainly an evaporation of capillary water occurred.

It was detected that, with increase of thermal damage, the specimens had a more ductile response. The heat treatments induced a change in the microstructure of the material, causing significant changes in its softening (post-peak) response. Furthermore, the ratio between the nominal strength of the damaged material and the nominal strength of the virgin material is size dependent. After thermal treatment, the material becomes less brittle (the intrinsic length increases), and the specimen size that is needed to determine the lower limit of the nominal strength for a given test geometry may decrease. Hence, evaluating the residual strength by considering identical specimens and applying the relations of classical beam theory may cause an underestimation of the effective or true residual strength of the material.

As presented in the Appendix A, the fracture parameters of a cohesive crack law can be obtained from the Size Effect Law (SEL). The SEL parameters of the three different considered concretes, such as G_f and c_f, can be evaluated. Knowing the parameter γ, which depends on the shape of the softening law and the ratio between G_F and G_f [16], the tensile strength, f_t, can be calculated. The average value $\gamma = 0.285$ is used as suggested in [17]. The specimens are characterized by a $\alpha_0 = 0.2$, the dimensionless energy release function $g(\alpha_0) = 0.5832$ and its derivative $g'(\alpha_0) = 3.2374$. The values of σ_N at failure are reported in Table 3 for the three series. As previously mentioned, the identification of the SEL parameters from the values in Table 3 can be done through linear regression, using the formulas in Eq. (6) and reported in Table 4, for the three concretes.

A linear cohesive crack law, characterized by the effective tensile strength f_t and initial fracture energy G_f, is considered. In this approach, the pre-peak behavior is assumed to be linear elastic and the nonlinearity before the peak is neglected, which leads to a small error for the reference (virgin) and 500 °C concretes. However, this approximation is assumed to be valid for the concrete treated at 750 °C as well. Table 4 reports the identified SEL parameters calculated according to the formulas in Eq. (7). These values indicate that (1) the equivalent crack extension increases significantly only for the higher thermal damage at 750 °C, and (2) the initial fracture energy increases for the intermediate thermal damage at 500 °C and decreases for higher thermal damage at 750 °C.

The value of total fracture energy, G_F, for the three concretes can be estimated as $2.5G_f$ [18]. The two parameters, f_t and G_f, are the true fracture properties of the concrete that should be compared in an experimental investigation on the effect of thermal damage. The tensile strength lowers to 46.1% and 11.85% for concrete at 500 °C and 750 °C, respectively. These values are quite close to the tensile strength recorded in the experimental tests (see Fig. 5). Using the two fracture parameters, f_t and G_f, in Eq. (5), the characteristic length is evaluated to be 171.4 mm, 198.3 mm and 460.7 mm for concretes without thermal treatment and treated up to 500 °C and 750 °C, respectively. This study agrees with the results of previous work [19] on a different type of concrete. The deterioration of the initial fracture energy for thermally damaged concrete in the residual condition is of fundamental impor-

Table 4
SEL parameters of concrete after different thermal treatment identified from the nominal strength of TPB tests.

Concrete	A (MPa^{-2})	C (mm^3/N^2)	σ_0 (MPa)	D_0 (mm)	G_f (N/mm)	c_f (mm)	f_t (MPa)
virgin	0.00041	0.111	3.007	271.21	0.0376	48.85	2.89
500 °C	0.00166	0.521	1.385	313.69	0.0763	56.51	1.33
750 °C	0.01291	9.391	0.326	728.83	0.0151	131.29	0.313

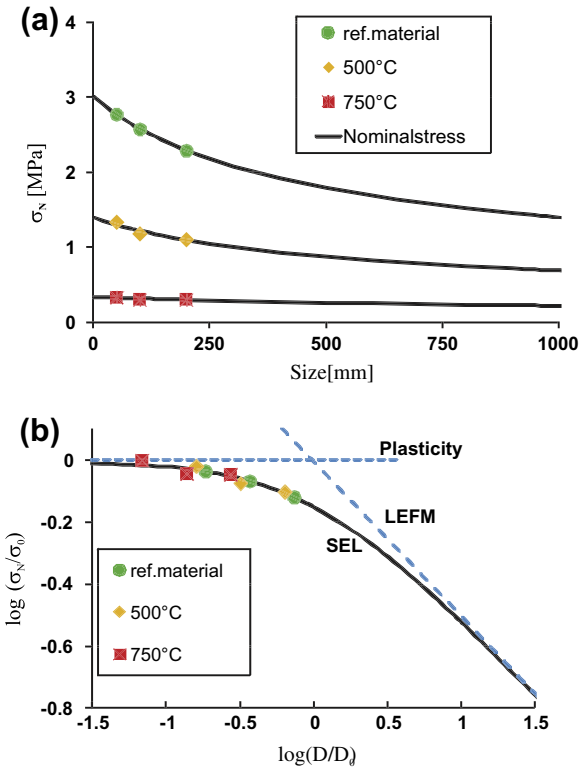

Fig. 11. Size effect plots: (a) influence of thermal treatment on the nominal strength and (b) change in mode of failure after thermal treatment.

tance from the design point of view with respect to the evaluation of the total fracture energy (among others [2,20]), since the initial fracture energy determines the maximum load of notched fracture specimens for normal-size as well as most concrete structures [18].

Fig. 11a presents the SEL curves for nominal stress as fitted to the experimental data points. Since the test results agree reasonably well with the SEL law they can be placed in one plot as shown in Fig. 11b. In this plot there is a significant shift of the data sets toward the left (to plasticity, i.e. a strength criterion) as the temperature increases and exceeds 500 °C. This means that fracture propagation becomes more ductile as the temperature becomes greater. Damage and energy dissipation are more distributed for higher temperatures of exposure. However, this result differs from that of Bažant and Prat (1988), who applied the size effect method to fracture specimens at different temperature in hot conditions but limited to 200 °C. The present study is focused on the residual properties of concrete after thermal treatment at different temperature, in which the influence of creep on fracture propagation [21,22] is much less marked with respect to hot conditions. The size of the fracture process zone can be also taken as the measure of brittleness or ductility: a material with a large process zone is more ductile.

A significant result from the present study, which confirms a previous one [19], is the increase of the fracture process zone (c_f) as the temperature (damage) increases. This implies that the material ductility, and consequently the ductility of the structural failure, increases due to thermal effect on the material microstructure. This phenomenon is more evident on the characteristic length l_1, which is five time larger for concrete at 750 °C with respect to the reference concrete. This phenomenon is also confirmed in the experimental tests in which the deformation field at the peak, depicted in Fig. 6, clearly reveals that the extension of damage is larger for higher temperature of exposure. This means that the volume, in which the energy is dissipated, increases due to the changing of the material microstructure and, consequently, from the macroscopic point of view, of its constitutive law.

An important distinction is in the pre-peak microcracking, which influences the strength of a specimen and the scaling of strength. It is important to realize that after heat treatment, the specimens have an altered behavior. In this context, an understanding of the failure process of the quasi-brittle material is needed for a correct interpretation of the experimental data. Therefore, experiments on specimens of different sizes should be conducted to find the intrinsic residual properties independent of specimen size. For example, the experiments should include: (a) appropriate monitoring to detect the characteristics of the microcracked volume at peak load and (b) specimens of different sizes, but geometrically similar, to identify a true residual strength of the damaged material, by taking into account the size effect on nominal strength.

The photocatalytic property characterizes this concrete mix for self cleaning and depolluting effects. In particular, on-going research shows that cement-based materials containing TiO_2 have a good response to urban pollution control [9]. Examples of pollutants that can be eliminated by the photocatalytic cementitious products are NO_x, SO_x, NH_3, CO, volatile organic carbons (VOCs) such as benzene and toluene, organic chlorides, aldehydes, and polycondensated aromatics. This study shows that after a thermal treatment at the temperature of 750 °C, the titanium dioxide (TiO_2) active phase anatase transforms to the inactive phase rutile, which in turn, produces the loss of the photocatalytic property.

5. Conclusions

The paper presents an investigation on the evolution of the mechanical and chemo-physical properties of a white high performance concrete (containing titanium dioxide) exposed to the elevated temperatures of 250, 500, and 750 °C. Based on the experimental evidence, the following conclusions can be drawn. With heat treatment to high (>500 °C) temperatures, profound and irreversible transformation in the material must be considered in an analysis of residual properties in bending. Testing thermally damaged specimens of similar geometry, the experiments showed that the population of microcracks evolves (in number and size of cracks) depending on thermal incompatibility of the constituents and the alterations in the material due to heating.

Crack propagation in concrete specimens with variable amounts of damage is accompanied by a process zone of variable size. Due to the heating scenario, a diverse evolution of residual strength with size occurs: i.e., the damage process detected in the specimens influences the mechanical properties. The characteristic length of concrete treated at 750 °C was five times larger than that of the reference concrete. This observation is supported by the shift in behavior on the size effect plot to the left, toward higher ductility. This means that fracture behavior becomes more ductile with increasing temperature of the thermal treatment. In addition, we observed that even in the elastic regime the damaged concrete responds in a different way depending on whether the external loads are tensile or compressive.

Generally speaking, the results showed that the existence of microcracks decreases the effective stiffness of the material, and the effective moduli further decrease as the microcrack density is increased. The behavior of this concrete after the thermal treatments is similar to the behavior of an ordinary concrete with limestone aggregate.

This study reveals that the photocatalytic property of this white concrete is preserved at least up to a temperature of 500 °C. Based on X-ray diffraction analysis, the thermal treatment at 750 °C showed a transformation of the active phase of titanium dioxide to an inactive phase, implying a loss of photocatalytic capability.

Acknowldgements

The authors wish to extend their gratitude to Dr. Gian Luca Guerrini of Italcementi Group for the great contribution concerning the experimental program. The authors are grateful to Mr. Stefano Citterio whose work for the M.S. thesis provided an important part of the results presented in this paper. Special thanks are due to Dr. Giovanni Muciaccia and to the technicians Daniele Spinelli, Tonino Cocco and Paolo Broglia, who supervised the student in setting up the experimental apparatus.

Appendix A. Size effect law

For specimens of the same geometry but different sizes and notch length a_0, the introduction of the concept of an effective crack of length $a_0 + c_f$ into the LEFM equation for the nominal stress at failure, after some mathematical manipulations and using the classical Irwin's relation, leads to the well known the Size Effect Law (SEL) of Bažant [23]:

$$\sigma_N = \sigma_0\left(1+\frac{D}{D_0}\right)^{-1/2} = \sqrt{\frac{EG_f}{g'(\alpha_0)c_f + g(\alpha_0)D}} \tag{3}$$

where

$$\sigma_0 = Bf_t \text{ and } D_0 = \frac{EG_f}{(f_tB)^2 g(\alpha_0)} = \frac{l_1}{B^2 g(\alpha_0)} \tag{4}$$

Here $\sigma_N = 4.2P_{max}/bD$ is the nominal strength of the considered 3 PB geometry, P_{max} is the maximum load, b is the specimen width; $\alpha_0 = a_0/D$ is the dimensionless notch length; $g(\alpha) = k^2(\alpha)$, where $k(\alpha) = K_I/\sigma_N\sqrt{D}$ is the dimensionless stress-intensity factor; E is the Young's modulus; D_0 is the transitional size; σ_0 is the nominal strength extrapolated to zero size ($D \to 0$) according to the classical size effect law, f_t is the direct tensile strength of material, B is a geometry constant depending on specimen geometry; c_f must be regarded as a constant independent of the size D. Furthermore, the parameter l_1 [24] represents the characteristic length of the material corresponding to the initial fracture energy, G_f, to be distinguished from characteristic length $l_0 = EG_F/f_t^2$ corresponding to the total fracture energy, G_F

$$l_1 = \frac{EG_f}{f_t^2} = B^2 g'(\alpha_0)c_f \tag{5}$$

Since in a plot $Y = 1/\sigma_N^2$ versus $X = D$, the size effect law appears as a straight line, $Y = AX + C$, the coefficients of the size effect law are fitted by using linear regression. Once the slope A and the intercept C have been evaluated, constants D_0 and $\sigma_0 = B f_t$ in Eq. (3) can be determined as

$$\sigma_0 = \frac{1}{\sqrt{C}} \text{ and } D_0 = \frac{C}{A} \tag{6}$$

Then the fracture energy, the effective process zone length, and the tensile strength of cohesive crack model can be obtained as

$$G_f = \frac{\sigma_0^2}{E} D_0 g(\alpha_0), c_f = D_0 \frac{g(\alpha_0)}{g'(\alpha_0)} \text{ and } f_t = \sqrt{\gamma\sigma_0 g'(\alpha_0)} \tag{7}$$

References

[1] Schneider U. Concrete at high temperatures – a general review. Fire Safety J 1988;13:55–68.
[2] Phan L, Carino N. Review of mechanical properties of HSC at elevated temperature. J Mater Civil Eng ASCE 1998;10:58–64.
[3] Phan L, Carino N. Effects of test conditions and mixture proportions on behavior of high-strength concrete exposed to high temperatures. Mater J ACI 2002;99:54–66.
[4] D.S. John, A. Poole, I. Sims, Concrete Petrography: A Handbook of Investigative Techniques, Butterworth-Heinemann, 1998, pp. 308–317.
[5] Alonso C, Fernandez L. Dehydration and rehydration processes of cement paste exposed to high temperature environments. J Mater Sci 2004;39:3015–24.
[6] Khoury G. Compressive strength of concrete at high temperatures: a reassessment. Cem Concr Res 1992;44:291–309.
[7] Biolzi L, Cattaneo S, Rosati G. Evaluating residual properties of thermally damaged concrete. Cem Concr Compos 2008;30:907–16.
[8] Cattaneo S, Biolzi L. Assessment of thermal damage in hybrid fiber-reinforced concrete. J Mater Civil Eng ASCE 2010;22:836–45.
[9] Guerini GL. Photocatalytic performances in a city tunnel in Rome: NO_x monitoring results. Construct Build Mater 2012;27:165–75.
[10] Castillo C, Durrani A. Effect of transient high temperature on high strength concrete. Mater J ACI 1990;87:47–53.
[11] Biolzi L, Cangiano S, Tognon G, Carpinteri A. Snap-back softening instability in high strength concrete beams. Mater Struct (RILEM) 1989;22:429–36.
[12] Popovics J. Analysis of the concrete strength versus ultrasonic pulse velocity relationship. Mater Eval 2001;59:123–9.
[13] Cattaneo S, Rosati G. Effect of different boundary conditions in direct tensile tests: experimental results. Mag Concr Res 1999;51:365–74.
[14] Biolzi L. Stress concentration factors in axisymmetric solids under imposed deformations. Meccanica 1987;22:19–26.
[15] Labuz J, Biolzi L. Experiments with rock: remarks on strength and stability issues. Int J Rock Mech Min Sci 2007;44:525–37.
[16] Bažant Z, Yu Q. Size-effect testing of cohesive fracture parameters and nonuniqueness of work-of-fracture method. J Eng Mech 2011;137:580–8.
[17] Yu Q, Le J, Hoover C, Bažant Z. Problems with Hu-Duan boundary effect model and its comparison to size-shape effect law for quasi-brittle fracture. J Eng Mech 2010;136:40–50.
[18] Bažant Z, Yu Q, Zi G. Choice of standard fracture test for concrete and its statistical evaluation. Int J Fract 2002;118:303–37.
[19] Di Luzio G, Muciaccia G, Biolzi L. Size effect in thermally damaged concrete. Int J Damage Mech 2010;19:631–56.
[20] Zhang B, Bicanic N. Fracture energy of high-performance concrete at high temperatures up to 450 °C: the effects of heating temperatures and testing conditions (hot and cold). Mag Concr Res 2006;58:277–88.
[21] Bažant ZP, Gettu R. Rate effects and load relaxation: static fracture of concrete. ACI Mater J 1992;89(5):456–68.
[22] Di Luzio G. Numerical model for time-dependent fracturing of concrete. J Eng Mech, ASCE 2009;135:632–40.
[23] Bažant ZP, Planas J. Fracture and size effect in concrete and other quasibrittle materials. Boca Raton (Florida): CRC Press; 1998.
[24] Cedolin L, Cusatis G. Identification of concrete fracture parameters through size effect experiments. Cem Concr Compos 2008;30:788–97.